Highly Stable 11-MUA Capped Gold Nanobipyramid for Refractive Index Sensing

Prajna N. Deviprasada and Rajeev K. Sinha*
Department of Atomic and Molecular Physics, LG-1, Academic Block 5, MIT Campus, Manipal Academy of Higher Education, Manipal 576104, Karnataka, India

***e-mail:** rajeev.sinha@manipal.edu

Abstract. Gold nanobipyramids (Au NBPs) are nanostructures with narrow plasmon resonances, which make them suitable for sensing applications. In the present work, Au NBPs of different aspect ratios were synthesized using a seed-mediated growth method by tuning the seed volume. The usual capping molecule CTAB was replaced by 11-mercaptoundecanoic acid (11-MUA), and the nanoparticle stability was studied. The 11-MUA capped NBPs were found to be more stable compared to the CTAB capped NBPs. The bulk refractive index sensitivities of all Au NBPs of CTAB and 11-MUA capped NBPs were measured using sucrose solutions of different weight percentages (0–30%). 11-MUA capped Au NBPs showed better refractive index sensitivity than CTAB capped Au NBPs. The NBPs of aspect ratio 3 showed maximum sensitivity of 353 nm/RIU.

Keywords: localized surface plasmon resonance (LSPR); gold nanobipyramids; refractive index sensing.

Paper #3580 received 13 Jan 2023; revised manuscript received 18 Feb 2023; accepted for publication 23 Feb 2023; published online 24 Mar 2023. doi: 10.18287/JBPE23.09.010308.

1 Introduction

The localized surface plasmon resonance (LSPR) is an optical phenomenon observed in metal nanostructures with dimensions much smaller than the wavelength of light. The phenomenon appears due to the resonant oscillation of the conduction electrons on the surface of nanostructures [1, 2]. The band maxima in the LSPR spectra are extremely sensitive to the refractive index (RI) of the surrounding medium [1, 2]. The RI sensitivity of metal nanostructures forms the basis of many cost-effective LSPR-based biosensors [1, 3]. Anisotropic nanoparticles are more suitable candidates for sensing applications due to their large surface charge polarizability and associated local field enhancement. This enables the LSPR sensing of small molecules to large biomolecules [4–7]. Several metal nanoparticles, such as gold, silver, copper, and platinum, show appreciable LSPR phenomena. However, nanoparticles of gold and silver have absorption bands in the visible spectral regions, making them widely used in sensing applications. Gold nanoparticles are comparatively more stable, biocompatible, and widely used in several biomedical applications [8–11].

Although the higher chemical and structural stability of Au nanostructures over Ag nanostructures make them preferable for LSPR sensing, the higher width of plasmon bands appears to be a limiting factor for their regular use. Among different shapes of gold nanoparticles, gold nanobipyramids (Au NBPs) shows narrow width of plasmon bands. Further, the wavelength tunability of the longitudinal plasmon band of Au NBPs is possible in the visible and near-IR spectral region by tuning their length and aspect ratio. The sharp edges in NBPs result in high field enhancement, making them highly suitable for biosensing applications [12, 13]. In the recent past, an appreciable amount of work has been performed on the synthesis of gold nanobipyramids. The bi-pyramidal shape of Au nanoparticles was first reported by Jana et al. [14]. Later, Liu and co-workers developed a synthesis method using CTAB as a surfactant [15]. Other than CTAB, capping agents like PVP [16], CTBAB [17], and sodium oleate as secondary surfactant [18] were also used to synthesize NBPs.

In the recent past, we have worked on the synthesis and evaluation of refractive index (RI) sensitivity of silver [19–22] and gold nanostructures [23]. In

continuation, here we report the synthesis and RI sensitivity of Au nanobipyramids. The replacement of cetyltrimethylammonium bromide (CTAB) in CTAB capped Au NBPs by 11-mercaptoundecanoic acid (11-MUA) is performed to improve the stability of the Au NBPs. The RI sensitivity of CTAB and 11-MUA capped Au NBPs were investigated using various concentrations of sucrose. Compared to nanosphere and nanorods, nanobipyramid shows better sensitivity and higher figure-of-merit, making them more suitable for LSPR-based sensing applications.

2 Materials and Methods

For the synthesis and conjugation of gold nanobipyramids, hydrogen tetrachloroaurate (III) hydrate ($HAuCl_4 \bullet 3H_2O$), cetyltrimethylammonium chloride (CTAC), cetyltrimethylammonium bromide (CTAB), 11-mercaptoundecanoic acid (11-MUA), nitric acid (HNO_3), silver nitrate ($AgNO_3$), and 8-hydroquinoline (HQL) were procured from Sigma Aldrich. L–ascorbic acid (AA) and sodium borohydride ($NaBH_4$) were purchased from Loba Chemie Pvt Ltd. and Spectrochem, respectively. All the chemicals were used as received.

3 Experimental Methods

3.1 Synthesis of Gold NBPs

Au NBPs were synthesized following the seed-mediated method reported earlier by Chateau et al. [24]. For the preparation of seed nanoparticles, 80 μL of 25 mM $HAuCl_4$ and 72 μL of 0.25 M HNO_3 were added to 8mL of 66 mM CTAC. The mixture was stirred at 1000 rpm for a few minutes, and 100 μL of 50 mM $NaBH_4$ in NaOH was added. The solution colour was changed to brownish orange. After one minute of stirring, 60 μL of 0.1 M citric acid was added, and the seed solution was heated at 85 ºC for 1 h in a water bath.

The growth solution was prepared using 20 mL of 46.5 mM CTAB, 200 μL of 25 mM $HAuCl_4$, 165 μL of 5 mM $AgNO_3$, and 255 μL of 0.4 M ethanoic HQL. Seed solutions of varying volumes (0.2, 1, and 1.6 mL) were added in three 25 mL glass beakers. Then, 20 mL of growth solution was added to each beaker and placed in a hot-air oven set at 85 ºC for 10 min.

3.2 Functionalization of Au NBP with 11-Mercaptoundecanoic Acid

The functionalization of NBPs was performed using the sodium borohydride method reported earlier [25]. Before functionalization, the excess precursors and other reagents were removed from the NBPs by centrifuging the colloidal solution at 8000 rpm for 15 min. The yellow supernatant was discarded, and the residue was re-dispersed in 10 mM CTAB solution. For functionalization, 1.5 mL of 100 mM $NaBH_4$ was added to 15 mL of CTAB-capped NBPs. The solution was kept undisturbed for one hour, and 800 μL of 10 mM 11 MUA was added. After overnight incubation, the excess of 11 MUA was removed from the colloidal solution through centrifugation at 8000 rpm for 12 min. The supernatant was discarded, and the NBPs were re-dispersed in water.

3.3 Characterization of Au Nanobipyramids

The synthesized Au NBPs were characterized using UV-Visible absorption spectroscopy and Field emission scanning electron microscopy (FESEM). The absorption spectra were recorded using our lab-built setup, explained elsewhere [20]. The FESEM images of Au NBPs were recorded in Carl Zeiss Gemini SEM 300 instrument. The FESEM samples were prepared by immobilizing the NBPs on a glass coverslip using (3-Aminopropyl) trimethoxysilane (APTMS). The aspect ratio of NBPs were calculated using ImageJ software [26].

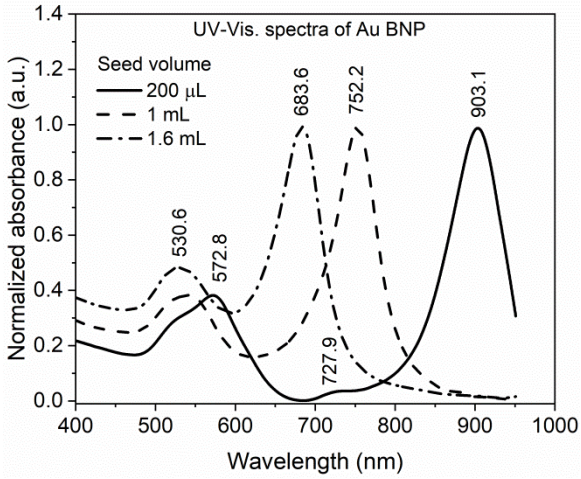

Fig. 1 Normalized absorption spectra of Au NBPs synthesized with different seed volumes.

4 Results and Discussions

4.1 Spectroscopic and Morphological Characterization of Au NBP

The NBPs are assumed as two pentagonal twinned bipyramids connected base to base. This structure forms due to the controlled growth of penta-twinned CTAC-capped seed particles in the growth solution. The growth solution is made up of gold precursor, stabilizing agent as CTAB, and shape directing agent as silver nitrate. The adsorption of silver as silver bromide on the surface of gold seeds leads to the anisotropic growth. The HQL as a mild reducing agent, reduces the reaction rate in the growth solution and favors the formation of the bipyramid structure of nanoparticles [27, 28].

The gold NBPs synthesized by the seed-mediated growth method [24] were characterized by UV-Vis spectroscopy using the lab-built setup [20]. The extinction spectra of Au NBP synthesized using seed volumes 200 μL, 1, and 1.6 mL are shown in Fig. 1.

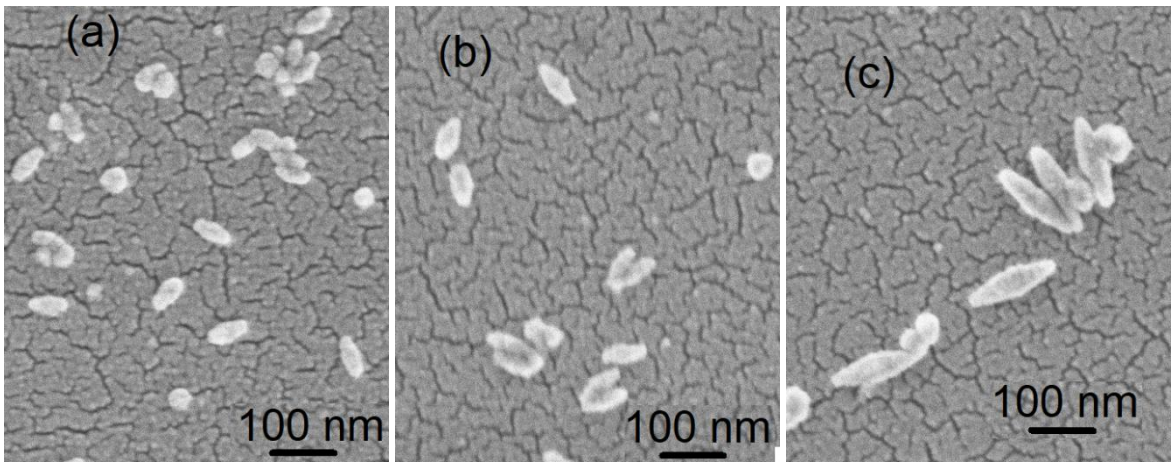

Fig. 2 FESEM images of 11-MUA capped gold nanobipyramids synthesized using (a) 1.6, (b) 1.0, and (c) 0.2 mL of seed volume.

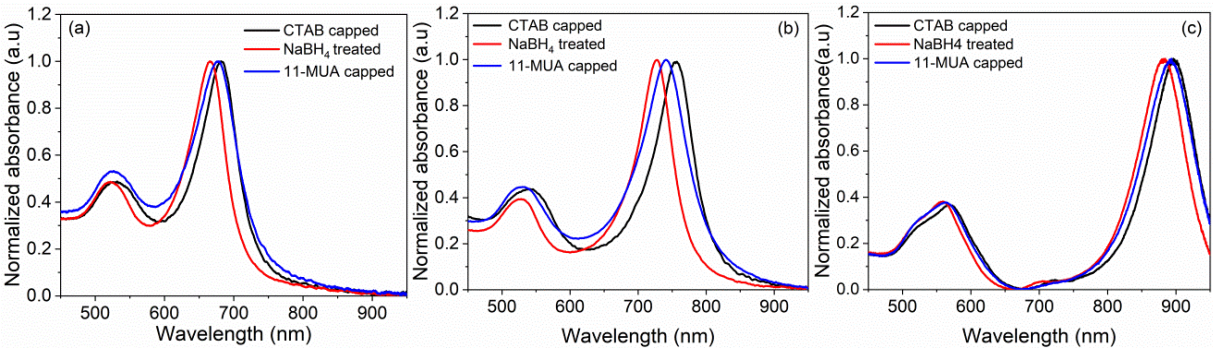

Fig. 3 Absorption spectra of NBPs as synthesized, after $NaBH_4$ treatment and after 11-MUA capping synthesized using (a) 1.6, (b) 1.0, and (c) 0.2 mL seed volume.

As it can be seen in the figure, for all three NBPs, two prominent features were observed, a transverse plasmonic band due to the oscillation of electrons along the short axis and a longitudinal plasmonic band due to the oscillation of electrons along the long axis [17]. The longitudinal plasmon band was observed towards the higher wavelength, and the transverse plasmon band towards the shorter wavelength. For seed volumes 200 µL, 1, and 1.6 mL, longitudinal plasmon bands appear at 903, 752, and 684 nm, respectively, whereas transverse band maxima were observed at the same position at 530.6 nm. The position of the longitudinal plasmon band towards longer wavelength signifies a higher length and aspect ratio of the NBP. Therefore, decreased seed volume resulted in longer NBP with a higher aspect ratio. An increase in the seed volume causes less availability of Au^{3+} ions per seed, resulting in a lower overall aspect ratio of NBPs [29]. The lower aspect ratio is responsible for the observed blue shifts in the longitudinal band position with an increase in the seed volume. For seed volume of 200 µL, two additional bands were seen at 572.8 and 727.9 nm. In a recent work, it is reported that as the length of NBP increases, the multipoles start appearing in the extinction spectrum [30]. The additional band observed at 572.8 nm could be due to the multipolar plasmon resonances, whereas the band at 727.9 nm could be due to a small number of by-products, such as gold nanorods [17].

The FESEM images of synthesized Au NBP are shown in Fig. 2. For imaging purpose, the NBPs were immobilized on a glass coverslip using 3-Aminopropyltrimethoxysilane (APTMS). As seen from the FESEM images, at 1.6 mL of seed volume, nanorice-shaped particles were formed (Fig. 2(a)). The bipyramidal shape of nanoparticles was improved by lowering the seed volume. More elongated bipyramids are formed for 200 µL seed volume, as shown in Fig. 2(c). The aspect ratios of these NBPs were calculated using ImageJ software, and the obtained aspect ratios were 2.0, 2.4, and 3, respectively.

4.2 Surface Functionalization and Stability of NBPs

Although CTAB acts as a stabilizing agent for the synthesized Au NBPs, a considerable blue shift in their longitudinal peaks was observed with time. Also, the

core of the nanoparticle is unapproachable for any biomolecular interactions due to the thick CTAB bilayers on the Au NBPs surface [31]. Therefore, CTAB must be replaced with suitable stabilizing agents which can retain the shape of the NBPs for a long time and make them more suitable for bioconjugation. The ligand exchange process using alkanethiol is a widely used method for the surface functionalization of nanoparticles [32]. While the alkanethiol, 11-MUA in present case, interacts with the NBPs through -SH head group, which has a strong affinity towards gold [13], the terminal carboxylic group (-COOH) can be modified using EDC/NHS chemistry [29] for bioconjugation.

The surface functionalization of Au NBPs by 11-MUA was performed using the sodium borohydride method reported by He et al. for the Au nanorods [25]. In the process, the CTAB-capped NBPs were treated with 50 mM $NaBH_4$. The absorption spectra of NBPs were recorded after 1 h and it is shown in Fig. 3(a–c). As can be seen, the addition of sodium borohydride shifts the longitudinal plasmon bands towards a lower wavelength. This could be due to a change in the refractive index at the nanoparticle surface appearing due to the replacement of CTAB by hydride ions [25]. The $NaBH_4$ modified NBPs were treated with 11-MUA followed by the investigation of absorption spectra. The addition of 11-MUA shifts the longitudinal bands towards a higher wavelength.

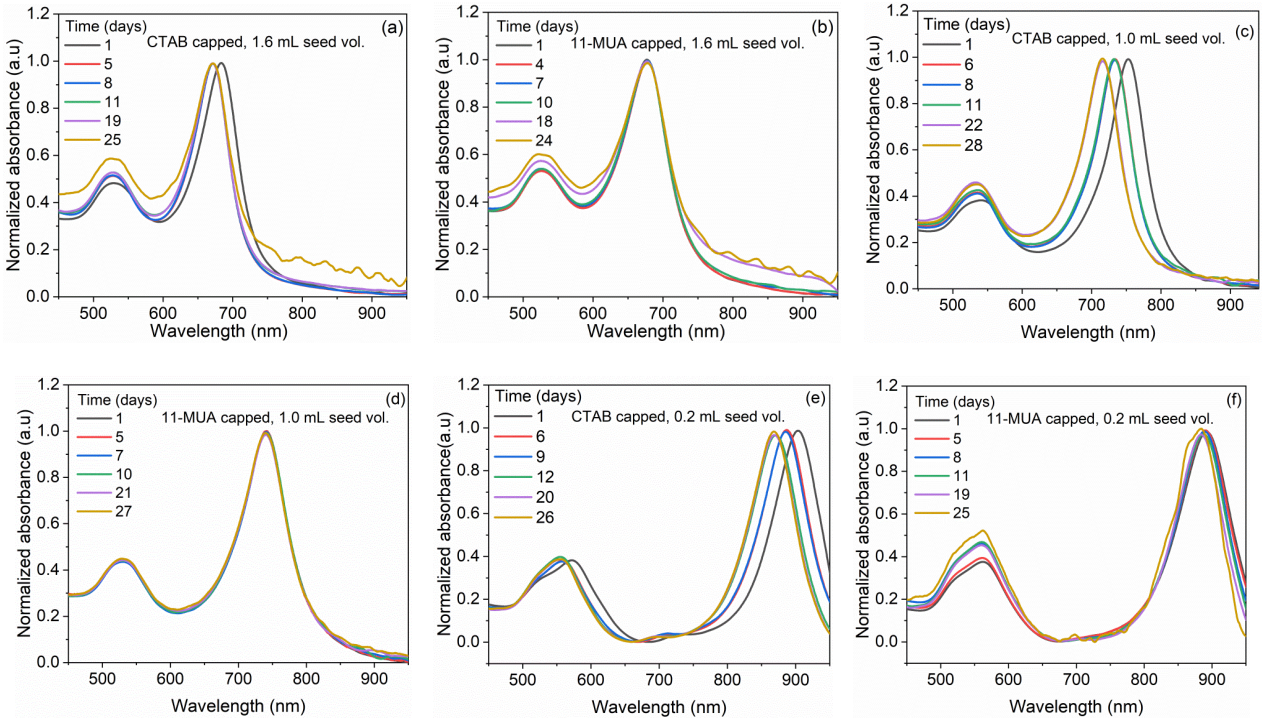

Fig. 4 LSPR band maxima of NBPs recorded on different days: CTAB capped NBPs synthesized using (a) 1.6, (c) 1, and (e) 0.2 mL of seed volume, and 11-MUA capped NBPs synthesized using (b) 1.6, (d) 1, and (f) 0.2 mL of seed volume.

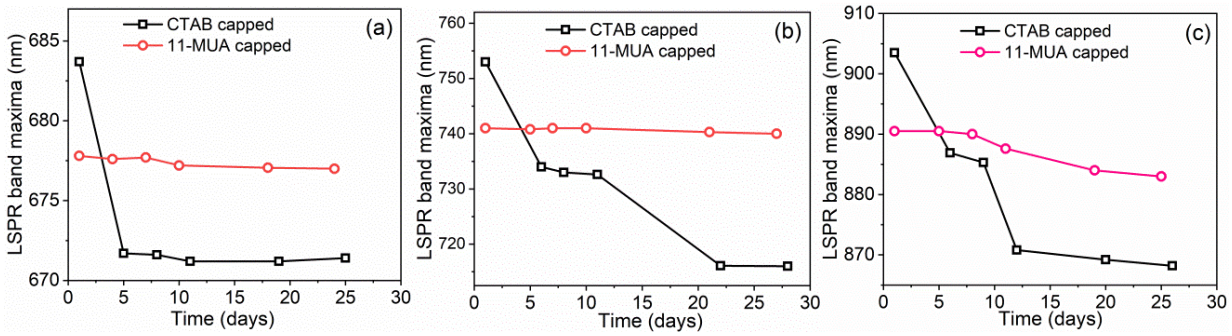

Fig. 5 Stability of CTAB capped, and 11-MUA capped Au NBPs with time synthesized using (a) 1.6 mL, (b) 1.0 mL, and (c) 0.2 mL of seed solution.

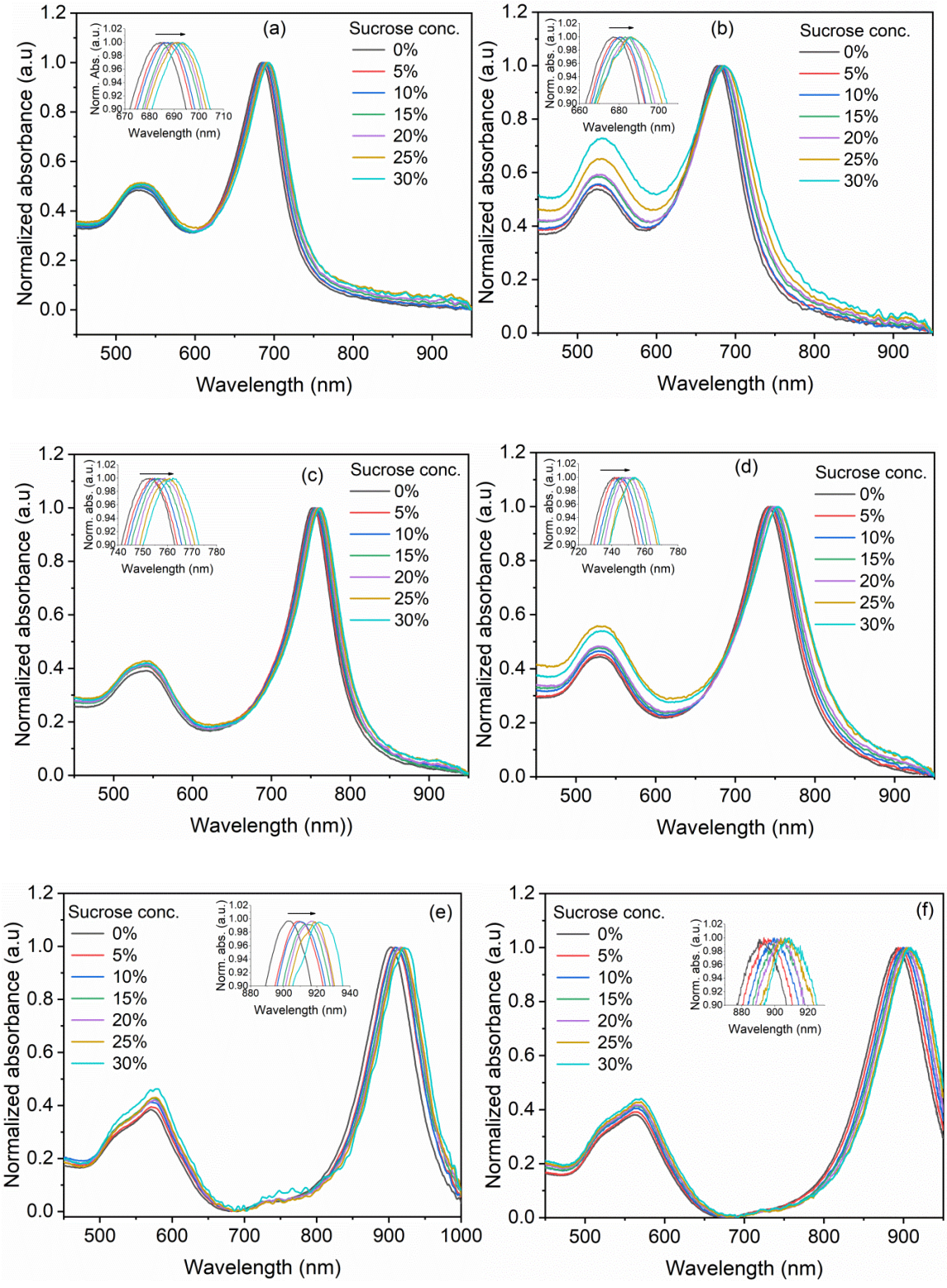

Fig. 6 LSPR absorption spectra of NBPs at different refractive indices of the medium (a), (c), and (e): CTAB capped NBPs synthesized using (a) 1.6, (c) 1.0, and (e) 0.2 mL seed volume; 11-MUA capped NBPs synthesized using (b) 1.6, (d) 1.0, and (f) 0.2 mL seed volume.

After overnight incubation, the NBPs solution was centrifuged to remove excess 11-MUA, and the absorption spectra were recorded. The redshifts in the longitudinal peaks were observed even after centrifuging, indicating the binding of 11-MUA molecules to the NBP surface. The longitudinal band maximum of as-prepared Au NBP in Fig. 3(a) is at 681 nm, which moved to 666 and 677 nm after $NaBH_4$

treatment and 11-MUA capping, respectively. The corresponding band positions in Fig. 3(b) are 752, 727, and 741 nm, and in Fig. 3(c), are 897, 882, and 892 nm.

The stability of both CTAB-capped and MUA-capped Au NBPs was also investigated. Fig. 4(a–f) shows the absorption spectra of NBPs recorded for more than three weeks, whereas Fig. 5(a–c) shows the variation in the longitudinal band maxima with time. As shown in Fig. 5(a–c), a gradual decrease in the LSPR peak position of CTAB-capped NBPs was observed with time which could be due to the decrease in the longitudinal size of bipyramids. However, in the case of 11-MUA-capped high aspect ratio NBPs, the observed trend is nearly linear. This indicated that the NBPs are highly stable in the presence of 11-MUA.

4.3 Refractive Index Sensitivity of NBPs

The refractive index sensitivity of synthesized Au NBP were investigated with sucrose solutions of varying weight/volume percentages (5–30%). Sucrose is selected as it is a highly water-soluble small molecule that provides the possibility of refractive index modulation of the solution in a controlled manner Fig. 6(a–f) shows the absorption spectra of Au NBPs with the variation of the sucrose concentration. Fig. 6(a, c, e) corresponds to Au NBP capped with CTAB, whereas Fig. 6(b, d, f) corresponds to the NBPs capped with 11-MUA. The inset in Fig. 6(a–f) shows the expanded region of longitudinal plasmon resonance band maxima. It is evident in all the LSPR spectra that the longitudinal plasmon band shifts towards red with an increase in the concentrations of sucrose. This indicates the sensitivity of the Au NBPs toward the refractive index of the surrounding medium.

Fig. 7(a–f) shows the variation of the longitudinal plasmon resonance band maxima with the change in the solution's refractive index. The refractive index values of sucrose were obtained from previously published works [33–35]. The experiment was repeated thrice for each concentration and for all three NBPs to ensure reproducibility and obtain the standard deviation. The experimental data points correspond to the average values of the band maxima position of three trials. The experimental data were fitted linearly to obtain the sensitivity of corresponding Au NBP. It was observed that the RI sensitivity of Au NBPs increases with their length and aspect ratio. Also, the 11-MUA capped NBPs show better sensitivity compared to the CTAB capped Au NBPs, which could be due to the variation in adsorbed layer length on the BPs surface because of the replacement of the CTAB bilayer by a single monolayer of MUA. The figure of merit (FOM) was also calculated using FOM = RIS/FWHM [17], which increases with an increase in the length and aspect ratio of the NBPs. Since the refractive index sensitivity depends on various factors like the refractive index of the medium, the length of adsorbed layer on the nanoparticle surface and the decay length, any change in one of these parameters would change the overall sensitivity of nanoparticles [36].

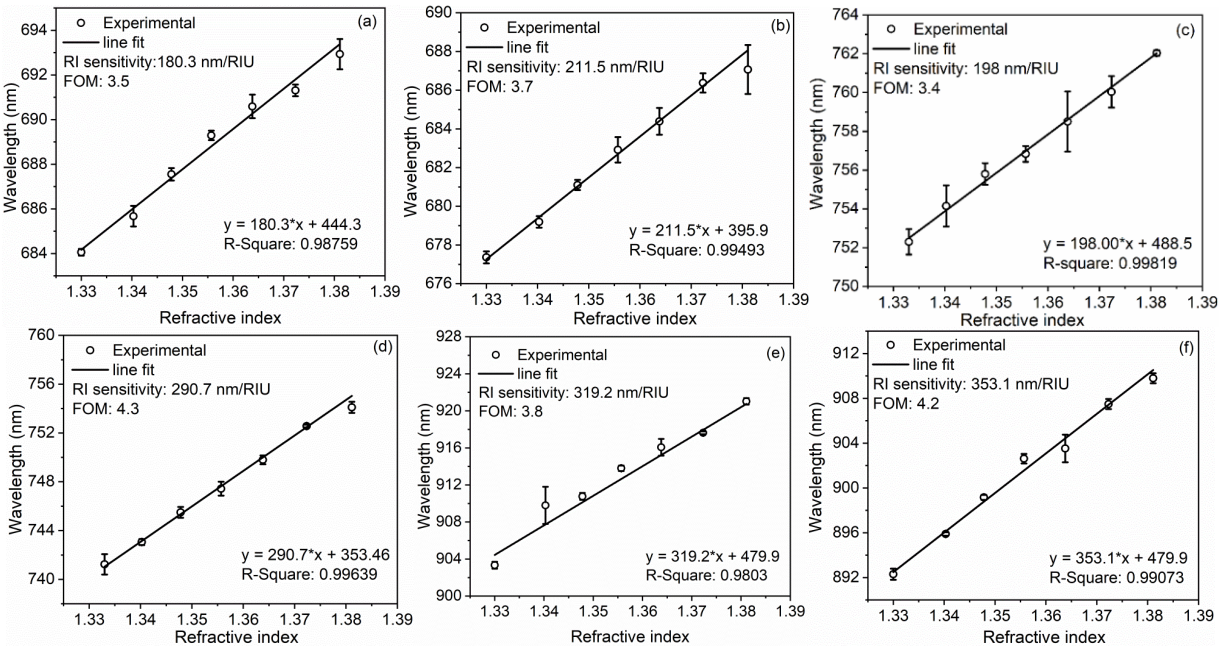

Fig. 7 Variation of longitudinal plasmon band maxima against the refractive index of the medium: CTAB capped NBPs synthesized using (a) 1.6, (b) 1.0, and (c) 0.2 mL seed volume; 11-MUA capped NBPs synthesized using (b) 1.6, (d) 1.0, and (f) 0.2 mL seed volume.

The obtained RI sensitivity of Au NBPs was compared with the RI sensitivity of Au nanospheres and Au nanorods. Table 1 lists the RI sensitivity of these nanostructures obtained in our earlier work as well as reported in other works. It is evident from the table that with comparable sizes, Au NBPs shows better RI sensitivity, which makes them more suitable for the RI sensitivity applications.

Table 1 Comparison of refractive index sensitivity of Au nanosphere, Au nanorods and Au NBPs.

Nanostructures	Size	RI sensitivity	Ref.
Au nanospheres	100 nm	180 nm/RIU	[37]
Au nanorods	2.7 AR	317 ± 8 nm/RIU	[23]
Au nanorods	2.7 AR	196 nm/RIU	[38]
Au nanobipyramids	3.0 AR	353 nm/RIU	This work

5 Conclusions

Gold nanobipyramids of different aspect ratios were synthesized using a seed-mediated growth method where the sizes of nanobipyramids were tuned using different seed solution volumes. The CTAB in CTAB capped Au NBPs was replaced by 11-MUA, which increased the stability of NBPs dramatically. The RI sensitivity of CTAB and 11-MUA capped Au NBPs were studied with different sucrose concentrations in water. It was found that the 11-MUA functionalized NBPs have better RI sensitivity and figure of merit (FOM) compared to the CTAB capped Au NBPs. Further, the RI sensitivity increases with an increase in the aspect ratio of Au NBPs. Refractive index sensitivity of 353 nm/RIU was obtained for NBPs synthesized using 0.2 mL of seed solution with an aspect ratio of 3.

Disclosure

The authors declare no conflict of interest.

Acknowledgments

Financial support from the Department of Science and Technology (DST) India under the project grant number IDP/BDTD/11/2019 is gratefully acknowledged. Prajna N D acknowledges the TMA Pai Ph. D. fellowship from the Manipal Academy of Higher Education (MAHE).

References

1. K. M. Mayer, J. H. Hafner, "Localized surface plasmon resonance sensors," Chemical Reviews 111(6), 3828–3857 (2011).
2. K. A. Willets, R. P. Van Duyne, "Localized surface plasmon resonance spectroscopy and sensing," Annual Review of Physical Chemistry 58, 267–297 (2007).
3. M. Chauhan, V. K. Singh, "Review on recent experimental SPR/LSPR based fiber optic analyte sensors," Optical Fiber Technology 64, 102580 (2021).
4. E. Petryayeva, U. J. Krull, "Localized surface plasmon resonance: Nanostructures, bioassays and biosensing - A review," Analytica Chimica Acta 706(1), 8–24 (2011).
5. H. Chen, L. Shao, K.C. Woo, T. Ming, H.Q. Lin, and J. Wang, "Shape-dependent refractive index sensitivities of gold nanocrystals with the same plasmon resonance wavelength," The Journal of Physical Chemistry C 113(41), 17691–17697 (2009).
6. J. Wang, H. S. Zhou, "Aptamer-based Au nanoparticles-enhanced surface plasmon resonance detection of small molecules," Analytical Chemistry 80(18), 7174–7178 (2008).
7. K. L. Kelly, E. Coronado, L. L. Zhao, and G. C. Schatz, "The optical properties of metal nanoparticles: the influence of size, shape, and dielectric environment," The Journal of Physical Chemistry B 107(3), 668–677 (2003).
8. S. Jung, K. L. Shuford, and S. Park, "Optical property of a colloidal solution of platinum and palladium nanorods: localized surface plasmon resonance," The Journal of Physical Chemistry C 115(39), 19049–19053 (2011).
9. P. Zheng, H. Tang, B. Liu, S. Kasani, L. Hung, and N. Wu, "Origin of strong and narrow localized surface plasmon resonance of copper nanocubes," Nano Research 12, 63–68 (2019).
10. J. Cao, T. Sun, and K. T. V. Grattan, "Gold nanorod-based localized surface plasmon resonance biosensors: A review," Sensors and Actuators B: Chemical 195, 332–351 (2014).
11. H. R. Hegde, S. Chidangil, and R. K. Sinha, "Review of synthesis and sensing applications of anisotropic silver and gold nanostructures," Journal of Vacuum Science & Technology B, Nanotechnology and Microelectronics: Materials, Processing, Measurement, and Phenomena 39(5), 050801 (2021).
12. T. H. Chow, N. Li, X. Bai, X. Zhuo, Lei Shao, and J. Wang, "Gold nanobipyramids: An emerging and versatile type of plasmonic nanoparticles," Accounts of Chemical Research 52(8), 2136–2146 (2019).

13. A. Campu, F. Lerouge, D. Chateau, F. Chaput, P. Baldeck, S. Parola, D. Maniu, A. M. Craciun, A.Vulpoi, S. Astilean, and M. Focsan, "Gold nanobipyramids performing as highly sensitive dual-modal optical immunosensors," Analytical Chemistry 90(14), 8567–8575 (2018).
14. N. R. Jana, L. Gearheart, and C. J. Murphy, "Seed-mediated growth approach for shape-controlled synthesis of spheroidal and rod-like gold nanoparticles using a surfactant template," Advanced Materials 13(18), 1389–1393 (2001).
15. M. Liu, P. Guyot-Sionnest, "Mechanism of silver (I)-assisted growth of gold nanorods and bipyramids," The Journal of Physical Chemistry B 109(47), 22192–22200 (2005).
16. X. Zhang, M. Tsuji, S. Lim, N. Mieyamae, M. Nishio, S. Hikino, and M. Umezu, "Synthesis and growth mechanism of pentagonal bipyramid-shaped gold-rich Au/Ag alloy nanoparticles," Langmuir 23(11) 6372–6376 (2007).
17. H. Chen, X. Kou, Z. Yang, W. Ni, and J. Wang, "Shape-and size-dependent refractive index sensitivity of gold nanoparticles," Langmuir 24(10), 5233–5237(2008).
18. Y. Xu, X. Wang, L. Cheng, Z. Liu, and Q. Zhang, "High-yield synthesis of gold bipyramids for in vivo CT imaging and photothermal cancer therapy with enhanced thermal stability," Chemical Engineering Journal 378, 122025 (2019).
19. H. R. Hegde, S. Chidangil, and R. K. Sinha, "Refractive index sensitivity of triangular Ag nanoplates in solution and on glass substrate," Sensors and Actuators A: Physical 305, 111948 (2020).
20. H. Hegde, C. Santhosh, and R. K. Sinha, "Seed mediated synthesis of highly stable CTAB capped triangular silver nanoplates for LSPR sensing," Materials Research Express 6(10), 105075 (2019).
21. H. R. Hegde, S. Chidangil, and R. K. Sinha, "Refractive index and formaldehyde sensing with silver nanocubes," RSC advances 11(14), 8042–8050(2021).
22. R. K. Sinha, "Surface-enhanced Raman Scattering and Localized Surface Plasmon Resonance Detection of Aldehydes Using 4-ATP Functionalized Ag Nanorods," Plasmonics 18, 241–253 (2022).
23. H. R. Hegde, S. Chidangil, and R. K. Sinha, "Refractive index sensitivity of Au nanostructures in solution and on the substrate," Journal of Materials Science: Materials in Electronics 33(7), 4011–4024 (2022).
24. D. Chateau, A. Desert, F. Lerouge, G. Landaburu, S. Santucci, and S. Parola, "Beyond the Concentration Limitation in the Synthesis of Nanobipyramids and Other Pentatwinned Gold Nanostructures," ACS Applied Materials & Interfaces 11(42), 39068–39076 (2019).
25. J. He, S. Unser, I. Bruzas, R. Cary, Z. Shi, R. Mehra, K. Aron, and L. Sagle, "The facile removal of CTAB from the surface of gold nanorods," Colloids and Surfaces B: Biointerfaces 163, 140–145 (2018).
26. C. A. Schneider, W. S. Rasband, and K. W. Eliceiri, "NIH Image to ImageJ: 25 years of image analysis," Nature Methods 9(7), 671–675 (2012).
27. S. Xu, W. Ouyang, P. Xie, Y. Lin, B. Qiu, Z. Lin, G. Chen, and L. Guo, "Highly Uniform Gold Nanobipyramids for Ultrasensitive Colorimetric Detection of Influenza Virus," Analytical Chemistry 89(3), 1617–1623 (2017).
28. D. Chateau, A. Liotta, F. Vadcard, J. R. G. Navarro, F. Chaput, J. Lermé, F. Lerouge, and S. Parola, "From gold nanobipyramids to nanojavelins for a precise tuning of the plasmon resonance to the infrared wavelengths: experimental and theoretical aspects," Nanoscale 7(5), 1934–1943 (2015).
29. C. Fang, G. Zhao, Y. Xiao, J. Zhao, Z. Zhang, and B. Geng, "Facile Growth of High-Yield Gold Nanobipyramids Induced by Chloroplatinic Acid for High Refractive Index Sensing Properties," Scientific Reports 6(1), 36706 (2016).
30. G. Weng, X. Shen, J. Li, J. Zhu, J. Yang, and J. Zhao, "Multipole plasmon resonance in gold nanobipyramid: Effects of tip shape and size," Physics Letters A 412, 127577 (2021).
31. J. Cao, E. K. Galbraith, T. Sun, and K. T. V. Grattan, "Effective surface modification of gold nanorods for localized surface plasmon resonance-based biosensors," Sensors and Actuators B: Chemical 169, 360–367 (2012).
32. J. Homola, "Present and future of surface plasmon resonance biosensors," Analytical and Bioanalytical Chemistry 377(3), 528–539 (2003).
33. OIML, "Automated Refractometers: Methods and Means of Verification," (2006).
34. D. F. Charles, "Refractive Indices of Sucrose-Water Solutions in the Range from 24 to 53% Sucrose," Analytical Chemistry 37(3), 405–406 (1965).
35. C. F. Snyder, A. T. Hattenburg, "Refractive indices and densities of aqueous solutions of invert sugar," National Bureau of Standards, Washington D. C. (1963).
36. L. Tian, E. Chen, N. Gandra, A. Abbas, and S. Singamaneni, "Gold Nanorods as Plasmonic Nanotransducers: Distance-Dependent Refractive Index Sensitivity," Langmuir 28(50), 17435–17442 (2012).
37. E. Martinsson, B. Sepulveda, P. Chen, A. Elfwing, B. Liedberg, and D. Aili, "Optimizing the refractive index sensitivity of plasmonically coupled gold nanoparticles," Plasmonics 9, 773–780 (2014).
38. L. P. F. Peixoto, J. F. L. Santos, and G. F. S Andrade, "Plasmonic nanobiosensor based on Au nanorods with improved sensitivity: A comparative study for two different configurations," Analytica Chimica Acta 1084, 71–77 (2019).